Three classes of one-dimensional, two-tile Penrose tilings and the Fibonacci Kronig-Penney model as a generic case

Mark Holzer*
Department of Physics, University of British Columbia, Vancouver, British Columbia, Canada V6T 2A6
(Received 11 February 1988)

We generalize the Fibonacci Penrose tiling to three classes of one-dimensional, two-tile Penrose tilings which can be obtained geometrically as well as recursively. From a numerical study of their spectral properties, we conclude that the Fibonacci case has the generic features of all three classes. As a model of epitaxial quasiperiodic superlattices we consider a Fibonacci Kronig-Penney model and give a physical picture relating structural to spectral properties.

Quasiperiodic systems have received much theoretical attention in recent years. Considerable progress has been made especially in one dimension by Ostlund *et al.*[1] and Kohmoto *et al.*[2–4] The simple scaling properties of the Fibonacci quasicrystal in particular, were shown to lead to a rich nonlinear dynamics in the form of the Kohmoto, Kadanoff, and Tang (KKT) renormalization scheme. While the issue as to whether quasicrystals occur naturally is not settled yet, man-made superlattices, in which thin films of semiconductor are stacked in a quasiperiodic manner, are indisputable physical realizations of one-dimensional (1D) quasiperiodic systems. Such superlattices have been grown epitaxially and their structural properties have been confirmed experimentally.[5–7] So far only Fibonacci lattices have been discussed in any detail in the literature. The Fibonacci lattice has golden-mean incommensurability, $(1+\sqrt{5})/2$, and is a special case of a two-tile Penrose tiling of the line. Here we generalize to three classes of two-tile Penrose tilings. From a study of their multifractal electronic spectra and corresponding wave functions we conclude that the Fibonacci case, despite its simplicity, has the generic features of all three classes.

In addition to the work by Kohmoto, we were motivated by a paper of Strömer *et al.*[8] in which, among other things, measurements of the Fermi surface of a periodic $GaAs/Ga_{1-x}Al_xAs$ superlattice were presented. What does a similar measurement on a quasiperiodic superlattice show? To answer this question, we explicitly calculate the one-electron energy spectrum and wave functions for periodic approximations to a quasiperiodic superlattice which we model, in the spirit of Ref. 8, by a Kronig-Penney-type potential. Combining the symmetries of two-tile Penrose tilings with a simple perturbative calculation of the band gaps, we give a physical picture relating structural to spectral properties. This paper is organized as follows.

In Sec. I we show how to obtain a class of two-tile Penrose tilings by geometrical construction. We give recursion relations which generate tiling sequences equivalent to the geometrically obtained ones for three classes of quadratic incommensurabilities. Such recursion relations, also known as inflation rules, embody the symmetries of the tiling. The three classes are generalizations of the Fibonacci case and we call them F classes.

In Sec. II we consider the spectral properties of the F classes. To this end we briefly review the theory of multifractals. We present numerical evidence, in the form of tight-binding spectra and wave functions for some members of these classes, which shows that the Fibonacci case has the generic features of all members of the F classes. We briefly discuss the KKT renormalization scheme and what we generalized thereof so far. We consider the possibility of labeling the states of the multifractal with quantum numbers which also label a sequence of inflation transformations under which the corresponding wave functions are invariant.

In Sec. III we turn to Fibonacci superlattices as modeled by a Kronig-Penney model. Explicit numerical results are presented and compared to a simple perturbative calculation of the band gaps leading to a physical picture relating structural to spectral properties. The calculation also gives a clear picture as to what we may consider to be the Fermi surface of such a superlattice.

I. GEOMETRICAL CONSTRUCTION AND SYMMETRIES OF TWO-TILE PENROSE TILINGS OF THE LINE

A class of 1D quasicrystals can be obtained geometrically by projecting from two dimensions as follows[9] (Fig. 1). Take the 2D lattice $L(x,y)=\sum_{n,m}\delta(x-an)\delta(y-bm)$. Draw the line $\Lambda=\{(x,y)\,|\,y-x\tan\theta\}$. If $\tan\theta\equiv\tau$ is irrational when x is measured in units of a and y in units of b, Λ is incommensurate with the lattice. In these units (which we shall call cubic units) choose $\pi/4<\theta<\pi/2$ and let τ be irrational. Now draw lines parallel to Λ through the lattice points $(-a,0)$ and $(0,-b)$ thus defining a strip Ω, the interior region bound by these lines. The 1D quasicrystal is then obtained by projecting the points $L\cap\Omega\cap\{(x,y)\,|\,x\geq 0,y\geq 0\}$ onto Λ. Let the lattice of projected points on Λ be denoted by $L(\zeta)=\sum_{j=0}^{\infty}\delta(\zeta-\zeta_j)$ with $\zeta_0=0$. Because $\Omega\cup\partial_\Omega$ contains only one conventional unit cell of $L(x,y)$, $[-a,0]\times[0,-b]$, Ω contains none. Consequently $\zeta_{j+1}-\zeta_j$ can only take on two values $l_A=b\sin\theta$ and

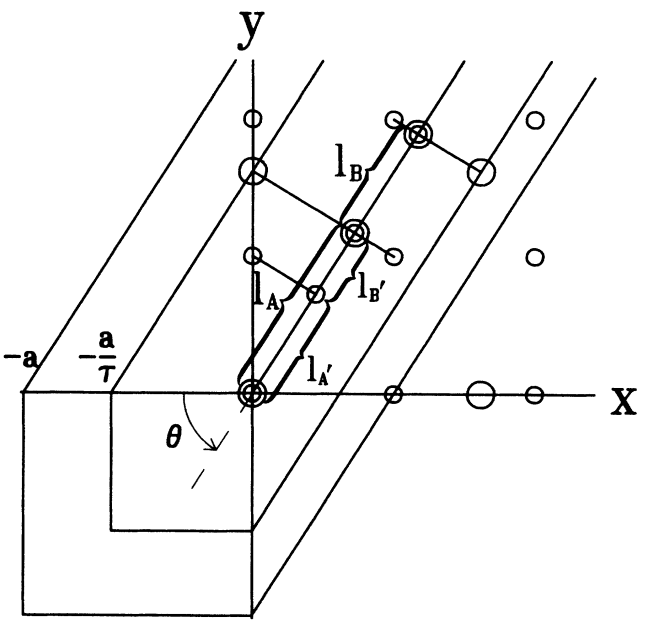

FIG. 1. The geometric construction of the Fibonacci lattice for $a=b$. One deflation step is shown.

$l_B=a\cos\theta$, the projections of the lattice vectors $[0,b]$ and $[a,0]$, respectively. $L(\zeta)$ is a Penrose tiling (i.e., an aperiodic tiling) of the line with the tiles l_A and l_B. The incommensurability $\tan\theta$ is seen to be the ratio of the number of A tiles to the number of B tiles. Further, we note that a B tile is always surrounded by A tiles and there can be at most $\mathrm{int}(1+\tau)$ A tiles side by side, where $\mathrm{int}(x)$ is the integer part of x. $L(\zeta)$ defines a sequence of tiles and hence a sequence of A's and B's which has a well-defined start because the origin of $L(x,y)$ is the only point of $L(x,y)$ on Λ. We denote the first P elements of this geometrically obtained sequence by $G^P(\tau)$.

While the geometrical construction of the tiling facilitates easy calculation of its Fourier transform (see Ref. 10 and Sec. III below), we would like to have an explicit analytical expression for $G^P(\tau)$ embodying the symmetries of the 1D quasicrystal. For example, it is well known that the above geometrical construction with $\tan\theta=(1+\sqrt{5})/2$, the golden mean, generates a sequence of tiles identical to that obtained by iterating the recursion relation $(A,B)\rightarrow(AB,A)$. What can we say about different incommensurabilities? Consider a recursion relation of the form

$$S_i^{k+1}(A,B)=\sum_{j=1}^{m} N_{ij}S_j^k(A,B)\ , \tag{1}$$

where N is a square matrix of positive integers, $S_i(A,B)$ stands for an ordered string of A's and B's and "addition" is ordered concatenation of strings. For example, if $S_1=ABA$, $S_2=BBA$ we would have $S_1+S_2=ABA,BBA$, $S_2+S_1\equiv BBA,ABA$, and $4S_1\equiv(S_1)^4\equiv ABA,ABA,ABA,ABA$. $S_i^k(A,B)$ defines the kth generation of a sequence of A's and B's which is obtained by iterating Eq. (1) k times with the initial conditions $S_i^0(A,B)$. The symmetry expressed by (1) is a set of m rules $S_i\rightarrow(S_1)^{N_{i1}},(S_2)^{N_{i2}},\ldots,(S_m)^{N_{im}}$ which tells us how to "inflate" pieces of the sequence $S_i^k(A,B)$ to obtain its next generation, $S_i^{k+1}(A,B)$. It is essentially a discrete conformal symmetry which, at least in the Fibonacci case, is known as *inflation symmetry*. We single out $S_1^k(A,B)$ as the kth generation tiling sequence of the 1D quasicrystal. If $P_{A_i}^k$ and $P_{B_i}^k$ denote the number of A's and B's contained in $S_i^k(A,B)$, then

$$P_{(A,B)_i}^{k+1}=\sum_{j=1}^{m} N_{ij}P_{(A,B)_j}^k \tag{2}$$

and $\tau=\lim_{k\rightarrow\infty}\tau_k$, where $\tau_k\equiv P_{A_1}^k/P_{B_1}^k$, is the solution of a polynomial with rational coefficients. What we seek then are N_{ij} and $S_i^0(A,B)$ such that τ is irrational and

$$S_1^k(A,B)=G^{P_1^k}(\tau)\ , \tag{3}$$

where $P_i^k\equiv P_{A_i}^k+P_{B_i}^k$. For future reference let $\sigma(\tau)\equiv\lim_{k\rightarrow\infty}(P_1^{k+1}/P_1^k)$ and note that $P_1^k\simeq\sigma^k$. Equivalence (3) is generally not satisfied; counterexamples are readily constructed. To date we were able to identify three classes of 2×2 recursion relations which do satisfy (3).

The first class is a straightforward generalization of the Fibonacci recursion relation which corresponds to $S_1=A$, $S_2=B$, $N_{11}=N_{12}=N_{21}=1$, and $N_{22}=0$. This recursion relation has an especially simple inflation symmetry which, in cubic units, has the geometric significance that the ratio of the length of the tiling corresponding to the kth iterate of A to the length of the tiling corresponding to the kth iterate of B is independent of k and equal to the incommensurability $\tau=l_A/l_B$. To preserve this symmetry a 2×2 matrix N must obey

$$N_{11}l_A+N_{12}l_B=\tau(N_{21}l_A+N_{22}l_B) \tag{4}$$

and τ is determined as a root of

$$\tau^2-\tau\,\mathrm{Tr}(N)+\det(N)=0\ , \tag{5}$$

where Tr denotes trace and det determinant. Comparing coefficients of (4) and (5) and setting $N_{12}=1$ so that B tiles are isolated, we arrive at the recursion relation

$$\begin{bmatrix}A'\\B'\end{bmatrix}=\begin{bmatrix}n&1\\1&0\end{bmatrix}\begin{bmatrix}A\\B\end{bmatrix} \tag{6}$$

and corresponding incommensurability

$$\tau(n)=\sigma=\tfrac{1}{2}[n+(n^2+4)^{1/2}]$$
$$=n+\cfrac{1}{n+\cfrac{1}{n+\cfrac{1}{n+\cfrac{1}{n+\cdots}}}}\ , \tag{7}$$

where the continued-fraction representation for τ is generated by the associated quadratic, Eq. (5). τ_k is seen to be given by the first k terms of this continued fraction.

Furthermore, we have $P^k_{B_1}=P^{k-1}_{A_1}$ and $P^k_{A_1}\equiv F_k=nF_{k-1}+F_{k-2}$ with $F_0=1$ and $F_1=n$. Explicitly,

$$F_k=[\tau^{k+1}+(-1)^k\tau^{-(k+1)}]/(n^2+4)^{1/2}\ .$$

When $n=1$ the numbers F_k are known as Fibonacci numbers. We call the $\tau(n)$ of Eq. (7) precious means, $\tau(1)$ and $\tau(2)$ conventionally being called the golden and silver mean, respectively (this nomenclature is consistent with the traditional assignment of the first few irrationals of this class to precious metals).

Class 2 generalizes a different form of the Fibonacci rule given by $S_1=A$, $S_2=BA$, $N_{11}=N_{12}=N_{21}=1$, and $N_{22}=2$ which has the symmetry $P^k_{B_2}=P^k_{A_1}$. The generalized recursion relation preserving this symmetry is given by

$$\begin{bmatrix} A' \\ (BA)' \end{bmatrix}=\begin{bmatrix} 1 & n \\ 1 & n+1 \end{bmatrix}\begin{bmatrix} A \\ BA \end{bmatrix} \tag{8}$$

and τ is the positive root of

$$\tau^2-\tau-1/n=0\ , \tag{9}$$

$$\tau(n)=\frac{1}{2}\left[1+\left[1+\frac{4}{n}\right]^{1/2}\right]$$

$$=1+\cfrac{1}{n+\cfrac{1}{1+\cfrac{1}{n+\cfrac{1}{1+\cdots}}}}\ . \tag{10}$$

Here too, τ_k is given by the first $(k+1)$ terms of the continued-fraction expansion of τ. We obtain $\sigma=\tau/(\tau-1)$.

Class 3 is the generalization of yet another form of the Fibonacci sequence: $S_1=ABA$, $S_2=BA$, $N_{12}=N_{21}=N_{22}=1$, and $N_{11}=2$. The symmetry which we generalize here is $P^k_{A_1}=P^k_{B_1}+P^k_{B_2}$. The generalized recursion relation preserving this symmetry is given by

$$\begin{bmatrix} (ABA)' \\ (BA)' \end{bmatrix}=\begin{bmatrix} n+1 & 1 \\ n & 1 \end{bmatrix}\begin{bmatrix} ABA \\ BA \end{bmatrix}\ . \tag{11}$$

The incommensurability τ satisfies

$$\tau^2+\tau(n-2)+1-2n=0\ ; \tag{12}$$

that is,

$$\tau(n)=\tfrac{1}{2}\{2-n+[(2-n)^2+4(2n-1)]^{1/2}\}$$

$$=0+\cfrac{2n-1}{n-2+\cfrac{2n-1}{n-2+\cfrac{2n-1}{n-2+\cdots}}}\ , \tag{13}$$

where the continued-fraction expansion is valid for $n>2$. Here τ_k bears no obvious relation to the truncated continued-fraction expansion (13). Furthermore, $\sigma=[\tau(n+2)+n+n\tau/(\tau+n-1)]/(\tau+1)$.

Figure 2 shows a plot of the three classes of quadratic irrationals $\tau(n)$ and summarizes the corresponding recursion relations. We note that as $n\to\infty$ the $\tau(n)$ approach rational values asymptotically and the quasicrystals have larger and larger periodic segments. Clearly the Fibonacci lattice is the simplest and most symmetric of all 1D quasicrystals. We call the subset of $L(\xi)$ such that $\xi_{j+1}-\xi_j=l_{A,B}$, the A (B) lattice, denoted by $L_{A,B}(\xi)=\sum_j\delta(\xi-\xi_{(A,B)_j})$. The Fibonacci lattice is the only 1D quasicrystal for which the A and B lattices are themselves 1D quasicrystals obeying the same recursion relation. The Fibonacci A and B lattices are given by

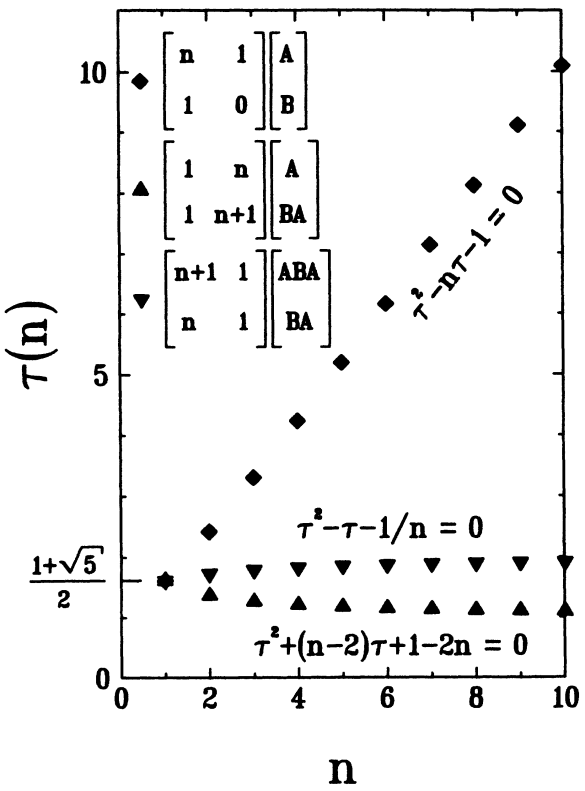

FIG. 2. Summary of the recursion relations considered in this paper and a plot of their incommensurabilities.

$$\xi_{j+1_A}-\xi_{j_A}=\begin{cases} l_A+l_B\equiv l_{A_A}\ , \\ \qquad\qquad \text{with } \xi_0=0\ , \\ l_A\equiv l_{B_A} \end{cases} \tag{14}$$

$$\xi_{j+1_B}-\xi_{j_B}=\begin{cases} 2l_A+l_B\equiv l_{A_B}\ , \\ \qquad\qquad \text{with } \xi_0=l_A\ , \\ l_A+l_B\equiv l_{B_B} \end{cases} \tag{15}$$

as we can see upon inflating once and twice, respectively. This fact has also been exploited by Dharma-wardana *et al.*[7]

It is not obvious that equivalence (3) is indeed satisfied by (6), (8), and (11). For class 1 a geometrical proof is already built into the way we obtained it. It is simply the fact that the inflation symmetry of this class can be made manifest geometrically by scaling both lattice constants of $L(x,y)$ by a factor of τ (Fig. 1). It is also straightfor-

ward to generalize the algebraic proof given by MacDonald[11] for the Fibonacci case, to all the precious means. If η_j denotes the vector from the point ζ_j on $L(\zeta)$ to the point of $L(x,y)$ from which it was projected, one proves that for the set $\{\zeta_j\}$, $\inf(\eta_j\cdot\hat{\mathbf{x}})=-a$ and $\inf(\eta_j\cdot\hat{\mathbf{y}})=-b$ assuming equivalence (3). We expect that such a proof can also be furnished for classes 2 and 3; we have satisfied ourselves with a numerical check.

From a number-theoretic point of view many questions remain. One is led to conjecture that a recursion relation of the form (2) exists for any irrational which is the root of a polynomial with rational coefficients. If the incommensurability is a transcendental, can one still speak of inflation symmetry? A different choice of Ω will generally result in a considerably more complicated situation; in particular, one will generally have more than two tiles. What are the corresponding recursion relations? Does some geometrical construction give sequences corresponding to a generic recursion relation of the form (2)? There clearly remains much to be understood, discovered, and proved.

II. MULTIFRACTAL SPECTRA, INFLATION SYMMETRY, AND QUANTUM NUMBERS

To study the problem of electrons in a 1D quasicrystal having inflation symmetry, it is natural to consider a sequence of periodic lattices. The kth element of this sequence has the kth inflation of (2) as its unit cell and we call it the kth periodic approximation (PA). As $k\to\infty$ the sequence of PA's converges to the 1D quasicrystal. In the kth PA, the unit cell contains P_1^k tiles and has length $L_k=P_{A_1}^k l_A+P_{B_1}^k l_B$. The potential in which the electron moves, is obtained by convolving the A (B) lattice of the 1D quasicrystal with some potential $V_{A,B}(\zeta)$ of finite range. The spectrum of the Hamiltonian, whether in a tight-binding or Kronig-Penney model, can conveniently be calculated by casting the problem in transfer matrix form, where the transfer matrix relates the wave function over a tile to the wave function over the next tile. For the kth PA, we can thus associate the sth tile of the unit cell, and therefore of $S_1^k(A,B)$, with a transfer matrix T_s which generally depends on the type of the sth tile (i.e., A or B) and the type of its neighbors. The net transfer matrix for a unit cell is then given by $M_{1_k}=\prod_{s=P_1^k}^{1} T_s=T_{P_1^k}T_{P_1^k-1}\cdots T_1$. Similarly we can define matrices M_{i_k} for all the sequences $S_i^k(A,B)$ of (2). The inflation symmetry (2) then implies a renormalization group equation for the M_{i_k}, relating the kth PA to the $(k+1)$th PA:

$$M_{i_{k+1}}=(M_{m_k})^{N_{i,m}}(M_{(m-1)_k})^{N_{i,(m-1)}}\cdots(M_{1_k})^{N_{i,1}} . \tag{16}$$

The energy E will belong to the spectrum of the kth PA, if $\lim_{n\to\infty}[M_{1_k}(E)]^n$ exists. That is, if

$$|x_k|\le 1 \quad \text{where } x_k\equiv\tfrac{1}{2}\mathrm{Tr}(M_{1_k}) . \tag{17}$$

Other physical problems[12] in 1D quasiperiodic geometry lead to similar conditions on the trace of M_{1_k}. By iterating (16) and finding the set of energies satisfying (17) at each step of the iteration, we obtain a sequence of spectra, corresponding to the sequence of PA's, which converges to the spectrum of the quasiperiodic Hamiltonian. Bands of the zeroth PA generally split up into P_k bands in the kth PA, where P_k is the number of distinct tiles per unit cell. Unless there is some incidental symmetry, $P_k=P_1^k$. We find that the sequences of spectra for members of the F classes converge to multifractal Cantor sets of zero Lebesque measure just as in the golden-mean case. Physically this is plausible if we think of the gaps as being due to recursively introduced periodic defects.

To characterize these multifractals, we follow Halsey *et al.*[13] First, we map the $k=0$ band onto the interval [0,1] and scale all other spectra accordingly. In the following discussion we refer to the rescaled bands. With the jth band of the kth PA, having a width (or "support") w_j, we associate a probability measure $p=1/P_k$ corresponding to the density of states integrated over this band, i.e., we normalize the number of states to 1. The scaling exponent α_j is then defined by $p=w_j^{\alpha_j}$. For the subset of $N(\alpha)$ bands which scale like α, and hence have width $w(\alpha)$, the density exponent $f(\alpha)$ is defined by $1=N(\alpha)w(\alpha)^{f(\alpha)}$. $f(\alpha)$ is an entropylike quantity: $f(\alpha)\sim\ln N(\alpha)$. As $k\to\infty$, $f(\alpha)$ converges to a spectrum of fractal dimensions which we expect to be a smooth function which then characterizes the multifractal. We obtain $f(\alpha)$ by a method which is essentially thermodynamic and motivated in Ref. 13. Here we only summarize the relevant results and point out some of the salient features: Let $q(\beta)$ be defined by the function

$$Z'_{P_k}=\sum_{j=1}^{P_k}\frac{p_j^q}{w_j^\beta}=1 . \tag{18}$$

We may consider q to be a free energy as can be seen from (18) by defining $Z=\sum_{j=1}^{P_k}w_j^{-\beta}$ so that $q=(\ln Z)/(k\ln\sigma)$. The entropylike variable $f(\alpha)$ is then obtained from $q(\beta)$ via a Legendre transform

$$f(\alpha)=q\frac{d\beta}{dq}-\beta,\quad \alpha=\frac{d\beta}{dq} . \tag{19}$$

Following Kohmoto,[14] we can make the thermodynamic analogy yet stronger by writing $w_j=e^{-\beta k\varepsilon_j}$. If we now define the entropy $S(\varepsilon)=(1/k)\ln\Omega(\varepsilon)$, where ε is the average of ε_j over Z at fixed β and $\Omega(\varepsilon)d\varepsilon$ is the number of bands whose "energy" ε_j lies between ε and $\varepsilon+d\varepsilon$, then it is straightforward to show that as $k\to\infty$

$$f(\alpha)=\frac{S(\varepsilon)}{\varepsilon},\quad \alpha=\frac{\ln\sigma}{\varepsilon} . \tag{20}$$

The maximum of $f(\alpha)$, $f(\bar{\alpha})$, can be shown to be the Hausdorff dimension of the multifractal, $\bar{\alpha}$ being its typical scaling exponent (the "thermal average" of the α's).

If one calculates $q(\beta)$ first from (18) and then obtains $f(\alpha)$ from (19), $f(\alpha)$ is a smooth function by construction for any k, whereas $S(\varepsilon)$ is expected to converge to a smooth function only as $k\to\infty$. Numerically, we find that the former method is more convenient and converges rapidly if we are indeed dealing with a well-defined Cantor set such as a tight-binding spectrum. The latter

appears to yield a more robust numerical procedure if we wish to obtain $f(\alpha)$ for a portion of a Cantor set or for a portion of a union of Cantor sets over a semi-infinite energy range such as we shall encounter in the Kronig-Penney model (see next section).

To investigate the spectral properties of the F classes we considered, for simplicity, the diagonal tight-binding model

$$\begin{bmatrix}\psi_{s+1}\\ \psi_s\end{bmatrix}=T_s\begin{bmatrix}\psi_s\\ \psi_{s-1}\end{bmatrix},\quad T_s\equiv\begin{bmatrix}E-V_s & -1\\ 1 & 0\end{bmatrix} \tag{21}$$

with $V_s=V_{A,B}$. We chose $V_A=1$ and $V_B=2$. For this model, Fig. 3 shows $f(\alpha)$ for the first three members of each of the three F classes. We see that as n increases the Hausdorff dimension increases slightly. The more periodic character of the lattice manifests itself in the increasing maximum value of α. To the accuracy of our calculations classes 2 and 3 have the same Hausdorff dimension for $n=2$ and 3. To get rapid convergence, we obtained $q(\beta)$ by setting $Z'_{P_k}=Z'_{P_{k+l}}$ and then calculated $f(\alpha)$ from (19). For some cases (indicated by a cross in Fig. 3) convergence for $\bar{\alpha}\ll\tilde{\alpha}<\alpha_{\max}$ was nonuniform. In the Fibonacci case where $\alpha_{\min}$ and $\alpha_{\max}$ are known analytically[4] (also see below), $f(\alpha)$ obtained from $Z'_{F_{13}}=Z'_{F_{15}}$ differs from that obtained from $Z'_{F_{13}}=Z'_{F_{17}}$ for $\alpha>\tilde{\alpha}$. The former overshoots $\alpha_{\max}$, the latter undershoots $\alpha_{\max}$ by roughly the same amount. The numerical $f(\alpha)$ curve appears to have a discontinuity of $\partial^2 f(\alpha)/\partial\alpha^2$ at $\tilde{\alpha}$. Preliminary calculations indicate that $\tilde{\alpha}\to\alpha_{\max}$ as $k\to\infty$. Figure 4 shows the magnitude of the on-site probability amplitudes $|\psi_n|$ at the center of the center tight-binding band for the first three members of the F classes in the PA's indicated in the figure. In the sense that (16) is always satisfied, the wave functions are clearly "critical" in nature and bear remarkable resemblance to those of the golden-mean case.

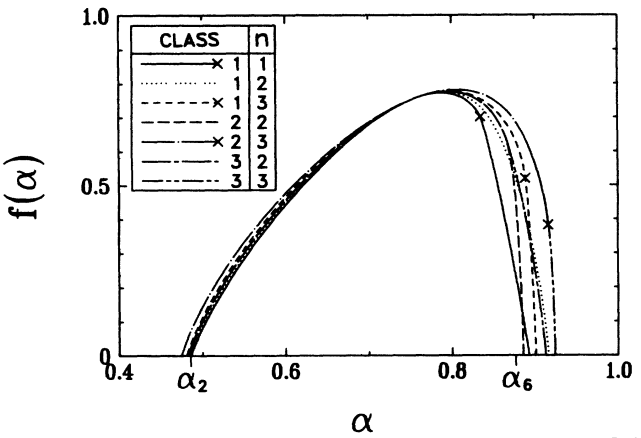

FIG. 3. $f(\alpha)$ vs α for the diagonal tight-binding model [cf. Eq. (21)]. The curves were computed from $Z'_N(q,\beta)=Z'_M(q,\beta)$. The (N,M) are, in the order of the table, (377,987), (239,577), (142,469), (71,256), (163,781), (41,571), (67,321). A cross indicates the maximum value of α for which uniform numerical convergence was obtained. α_2 and α_6 are the analytically obtained values for $\alpha_{\min}$ and $\alpha_{\max}$ in the Fibonacci case (class 1, $n=1$).

For the precious means (16) is particularly simple:

$$M_{k+1}=M_{k-1}M_k^n\ , \tag{22}$$

where $M_k\equiv M_{k_1}$. One can readily show that the traces of 2×2 matrices of unit determinant obeying (22) obey a recursion relation themselves. For $n=1$ we have

$$x_{k+2}=2x_{k+1}x_k-x_{k-1} \tag{23}$$

as first pointed out by KKT,[2] who discovered that (23) forms a 3D map $(x,y,z)\to(y,z,2yz-x)$ on the invariant manifold $I=x^2+y^2+z^2-2xyz-1$. Note that the 3D map conserves volume. Area on the invariant manifold is, however, not conserved except on n-cycles of the trace map. For $I<0$, the manifold I consists of a central compact part and four infinite sheets.[2,3] When $I=0$, the infinite sheets join the central part through four bottlenecks which widen with increasing I. When $I<0$ trace-map orbits starting on the compact part will obviously remain there. For $I>0$ they can escape over the bottlenecks, where the size of a bottleneck, and hence I, controls the rate of escape. Whether or not one sits in a band of the kth PA, for fixed I, is a function of the initial conditions for the KKT map, $(x,y,z(x,y,I))$. The set $\{x,y,z(x,y,I)\}$, such that $|x_k|\le1$ at fixed I, forms the kth approximation to a 2D multifractal on I (Fig. 5).

An algorithm for generating the trace maps of the other precious means is given in the Appendix. Invariants for these, if they exist, still remain to be found. The scaling exponents α_n for states of the multifractals corresponding to n-cycles of these trace maps can then be obtained analytically by linearizing the trace maps about these cycles. (See *Note added in proof.*)

If the symmetries of the 1D quasicrystal are expressible by an inflation relation of the form (2), it is natural to label the eigenstates of the Hamiltonian by an infinitely long sequence of n-ary digits, where $n=\text{int}(1+\sigma)$. Suppose there are P_1^k bands. If their eigenfunctions were exponentially localized, an unambiguous assignment of lattice sites to bands would be possible. Here, however, the wave functions are critical and hence not clearly associated with any lattice site in particular. While there may still be a natural way to make the assignment, here we arbitrarily map the tiling sequence S_1^k onto the bands in order from lowest to highest energy. If we consider the bands of the kth PA as mother states of the $\sim\sigma P_1^k$ daughter states of the $(k+1)$th PA, we can assign one integer $m\in\{0,\ldots,n-1\}$ to each daughter state according to the following rule: We label the sth element of S_1^1 (the daughter states) by $m=(s-1)\bmod n$ and assign it to the $[(s-m-1)/n+1]$th element of S_1^0 (the mother state). This assignment is then to be preserved as (2) is iterated. This procedure, which we illustrate in Fig. 6 for the silver-mean spectrum of (21), defines a family tree or n-furcation sequence for the daughter states. The n-ary quantum number is then simply the sequence of assignments m at each inflation step defining a branch of the family tree. With the proper assignment of tiles to bands, it should be possible to identify the n-ary quantum number with a sequence of inflation steps and reshufflings of parts of the corresponding wave function under which

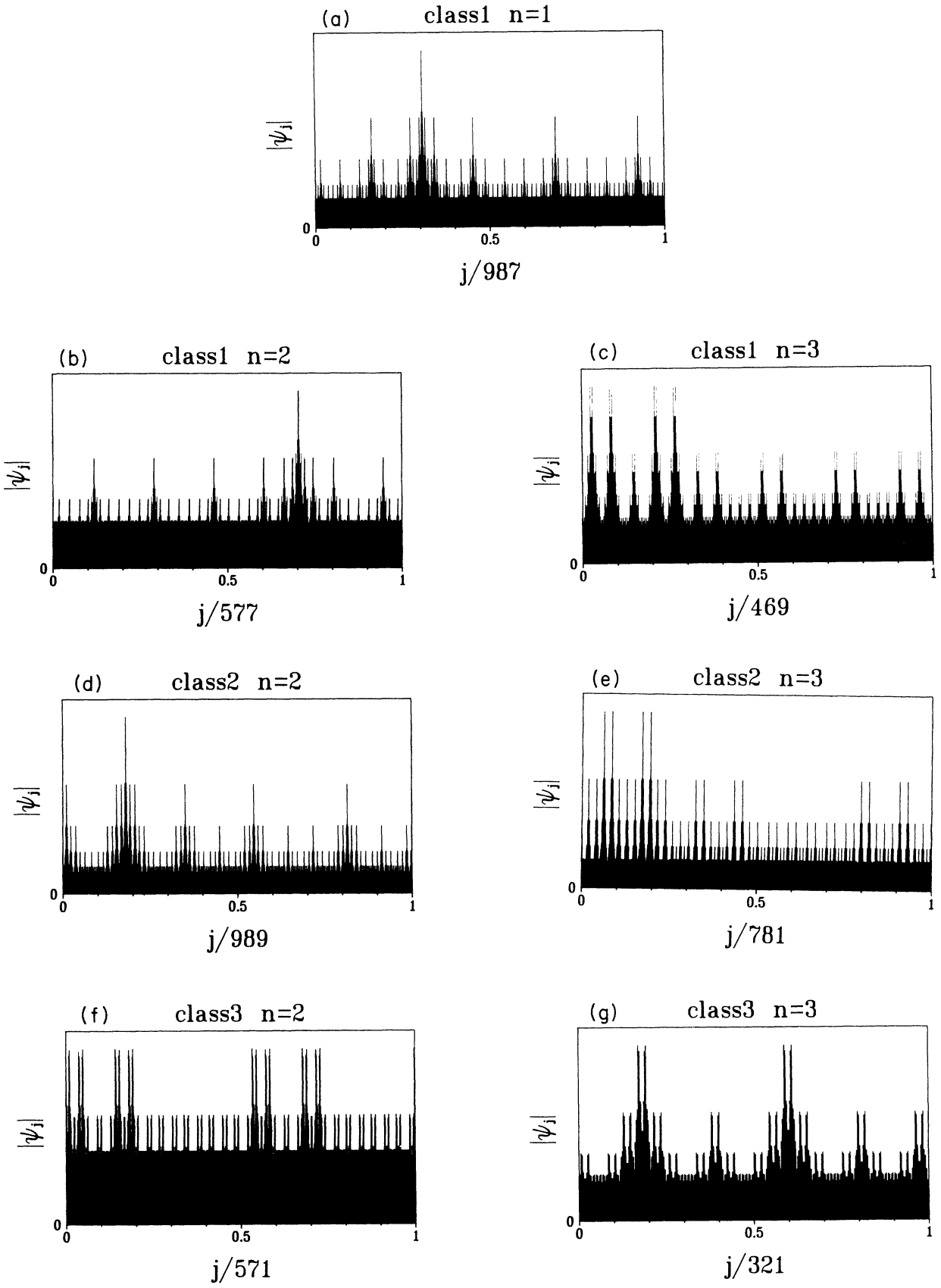

FIG. 4. The magnitude of the on-site probability amplitudes for the center states of the diagonal tight-binding model [cf. Eq. (21)].

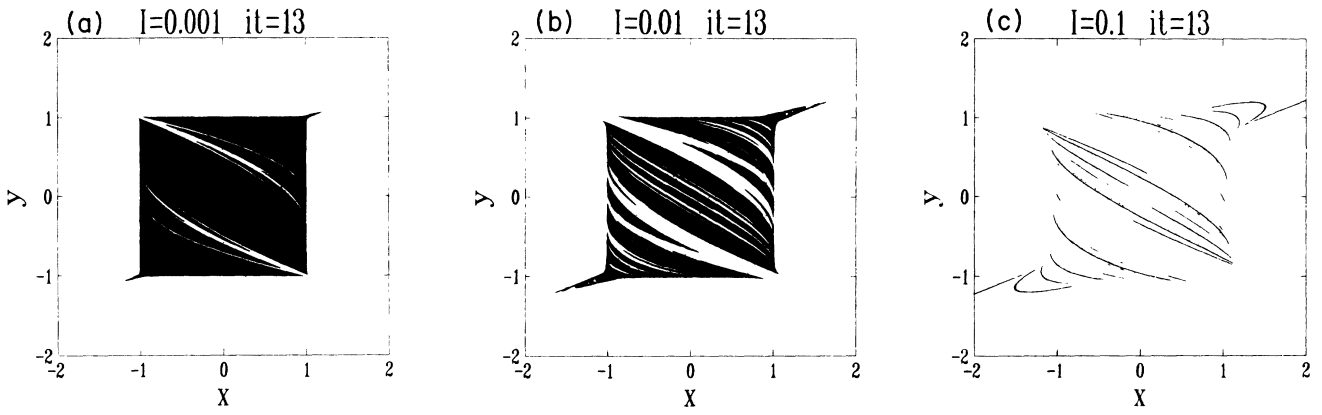

FIG. 5. The set $\{(x,y,z(x,y,I))\,|\,z>0\}$ of the golden-mean trace map which has not escaped after 13 iterations is shown for the values of I is indicated. (Actually the subset which falls on a 4000×4000 grid covering $[-2,2]\times[-2,2]$.) The rate of escape is seen to be governed by I.

the wave function is invariant. In the Fibonacci case such an invariance has been exhibited for the center and edges of the tight-binding Cantor spectrum.[3] There, however, the invariance is trivial as the wave functions are fractal. The general case of an arbitrary state needs to be elucidated still. In any case any well-defined assignment should make the sequence of spectra amenable to an analysis in terms of a mother to daughter ratio function which, as pointed out by Feigenbaum *et al.*,[15] allows one to map the system onto an Ising model. Such an analysis has yet to be carried out for the quasiperiodic electron problem.

III. THE FIBONACCI-KRONIG-PENNEY MODEL AND A PHYSICAL PICTURE CONNECTING STRUCTURAL AND SPECTRAL PROPERTIES

In approximating a GaAs/$Ga_{1-x}Al_xAs$ superlattice by a Kronig-Penney (KP) potential, one assumes that the electrons have an effective mass $m^*=0.0667m_e$, move in a potential of square barriers ($Ga_{1-x}Al_xAs$) and square wells (GaAs) perpendicular to the layers, and are free parallel to the layers. (The barrier height is controlled by the aluminum concentration.) We are thus left with an essentially 1D problem which we will analyze below.

A quasiperiodic Kronig-Penney potential is obtained by convolving the A (B) lattices with the pulses $V_{A,B}(\zeta)=V_{A,B}$ if $\zeta\in(\delta,w_{A,B}+\delta]$ and zero elsewhere, where $0<(w_{A,B}+\delta)<l_{A,B}$. Given the incommensurability, the two-tile KP potential is thus defined by the eight parameters $w_{A,B}$, $\delta_{A,B}$, $d_{A,B}$, and $V_{A,B}$.

Consider a string of KP pulses. The solution to the Schrödinger equation in the well regions between pulses is given by $C_ne^{ik\zeta}+D_ne^{-ik\zeta}$, where $k=(2m^*E/\hbar^2)^{1/2}$. The amplitude in front of barrier $n+1$ is related to the amplitude in front of barrier n by

$$\begin{bmatrix}C_{n+1}\\D_{n+1}\end{bmatrix}=\begin{bmatrix}e^{ikd_n}&0\\0&e^{-ikd_n}\end{bmatrix}\begin{bmatrix}1/t^*&r/t\\r^*/t^*&1/t\end{bmatrix}\begin{bmatrix}C_n\\D_n\end{bmatrix}\equiv\begin{bmatrix}T_n\end{bmatrix}\begin{bmatrix}C_n\\D_n\end{bmatrix}, \tag{24}$$

where t and r are the transmission and reflection coefficients of barrier n and d_n is the sum of the width w_n of barrier n and the width of the well following it.

For our kth-generation Kronig-Penney quasicrystal, Bloch's theorem reads

$$\tfrac{1}{2}\mathrm{Tr}(M_k)=x_k(E)=\cos(KL_k) \tag{25}$$

for crystal momentum K. From now on we consider only the Fibonacci case for simplicity and, as discussed in Sec. II, without loss of any important features. Accordingly, we calculate x_k by iterating the golden-mean trace map with the initial conditions $x=\frac{1}{2}\mathrm{Tr}(T_B)$, $y=\frac{1}{2}\mathrm{Tr}(T_A)$, and $z=\frac{1}{2}\mathrm{Tr}(T_BT_A)$. Explicitly,

$$\begin{aligned}&x=\cosh(\lambda_A)\cos(\varphi_A),\quad y=\cosh(\lambda_B)\cos(\varphi_B),\\&z=\cosh(\lambda_A)\cosh(\lambda_B)\cos(\varphi_A+\varphi_B)+|\sinh(\lambda_A)\sinh(\lambda_B)|\cos(k\Delta),\\&I=\cosh^2(\lambda_A)\cos^2(\varphi_A)+\cosh^2(\lambda_B)\cos^2(\varphi_B)+[|\sinh(\lambda_A)\sinh(\lambda_B)|\cos(k\Delta)-\cosh(\lambda_A)\cosh(\lambda_B)\sin(\varphi_A)\sin(\varphi_B)]^2\\&\quad-\cosh^2(\lambda_A)\cosh^2(\lambda_B)\cos^2(\varphi_A)\cos^2(\varphi_B)-1,\end{aligned} \tag{26}$$

where

$$t_{A,B}=|t_{A,B}|e^{i\chi_{A,B}},\quad \cosh(\lambda_{A,B})\equiv\frac{1}{|t_{A,B}|},\quad \varphi_{A,B}\equiv kd_{A,B}+\chi_{A,B},\quad \Delta\equiv d_A-d_B\ .$$

Notice that I is not positive definite. Numerically, we find that for some parametrizations of the KP potential, the invariant I is negative for energies below the ground state. Because we may view iterating (1) as introducing periodic defects in a recursive manner, we generally expect new gaps to appear with each iteration. In this sense, the essential physics of the quasiperiodic electron problem demands that trace-map orbits be able to escape and thus the initial conditions for the trace map which make $I<0$ for sufficiently low energies must lie on the infinite sheets of I which lie outside $x^2+y^2+z^2=3$. Equation (25) is the dispersion relation for the KP bands of the kth PA. Wave functions are obtained by propagating an eigenvector of M_k through the unit cell using the elementary transfer matrices (24) and matching boundary conditions at the barriers.

Typical lattice parameters of relevance to experiments are barrier heights of the order of 100 meV and well and barrier widths of the order 10–100 Å. We performed explicit numerical calculations for the lattice

$$(w_A,\delta_A,d_A,V_A,w_B,\delta_B,d_B,V_B)$$
$$=(17\text{ Å},0{,}59\text{ Å},134\text{ meV},17\text{ Å},0{,}59/\tau\text{ Å},134\text{ meV}),$$

which we shall refer to as the G lattice. The band structure converges to a multifractal Cantor set as $n\to\infty$ (Fig. 7). Figure 8 shows the scaling exponents $\varepsilon_j=-\frac{1}{17}\ln\Delta E_j$ for the 17th PA, where ΔE_j is the width of the jth band in meV. From this set of scaling exponents we obtained the entropy function $S(\varepsilon)$ and calculated spectra $f(\alpha)$ from (20) (including finite-k corrections) for the spectrum up to energy E (Fig. 9). With increasing E, $\alpha_{\max}$ increases and the Hausdorff dimension approaches 1. This agrees with one's intuition that the more energetic the electrons are, the more free-electron-like they become despite the fact that as $k\to\infty$ the Lebesque measure of the spectrum is expected to go to zero for arbitrarily high energies.

Figure 7 shows that the KP bands form clusters, the nth cluster containing F_n bands. Each cluster, in turn, resembles the band structure obtained from a tight-binding model. To understand this intuitively, we calculate the size of the gaps as obtained from simple two-level degenerate perturbation about free-electron states. The well-known result is that the nth gap ΔE_{g_n} is given by $\Delta E_{g_n}=2U_{nK_{BZ}}$, where U_k is the Fourier transform of the potential and $K_{BZ}=2\pi/L$. Using the geometrical construct for the infinite lattice $L(\zeta)$, Zia and Dallas[10] obtain its Fourier transform

$$L(k_\zeta)=i\frac{\sqrt{2\pi}}{ab}\sum_{n,m}\frac{e^{-ip_{nm}a\sin\theta}-e^{ip_{nm}b\cos\theta}}{p_{nm}}\delta(k_\zeta-k_{nm}),\tag{27}$$

where

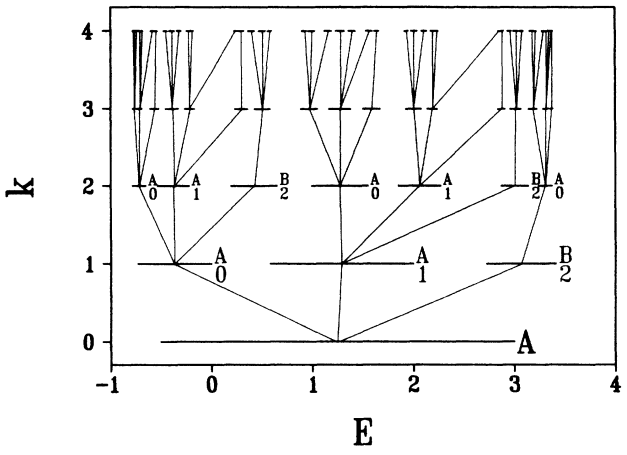

FIG. 6. n-furcation tree for the tight-binding bands of the silver-mean tiling. The rules of construction are given in the text.

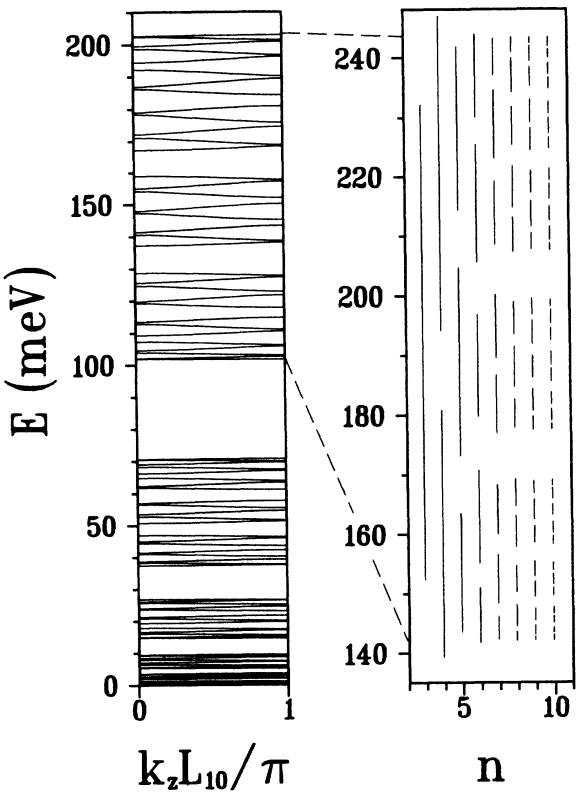

FIG. 7. Left-hand side: the band structure of the 10th PA to the G lattice. For energies below approximately 100 meV, the cluster structure looks approximately the same on a scaling $E\to E/\tau^2$. E is measured with respect to the system ground state which is 40.5 meV above the free-electron ground state. Right-hand side: the evolution of the indicated band cluster as we go to higher PA's labeled by n. The bands converge to a multifractal Cantor set. E is measured with respect to the free-electron ground state. (The ground-state energy depends on n.)

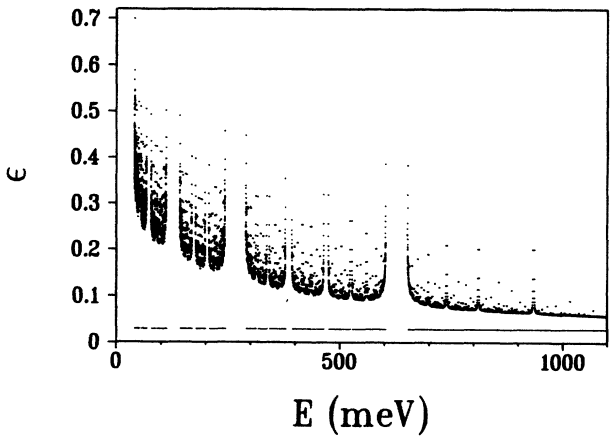

FIG. 8. The scaling exponents $\epsilon_j = -\frac{1}{17}\ln(\Delta E_j)$ vs E for the 17th PA to the G lattice. ΔE_j is the width of the jth band centered at energy E. The horizontal dashes are the bands themselves.

$$p_{nm} = 2\pi\left[\frac{m}{b}\cos\theta - \frac{n}{a}\sin\theta\right],$$
$$k_{nm} = 2\pi\left[\frac{n}{a}\cos\theta + \frac{m}{b}\sin\theta\right]. \tag{28}$$

The kth PA of $L(\zeta)$ is the periodic extension $Q_{p_k}(\zeta)$ of $Q(\zeta)=L(\zeta)g(\zeta)$, where $g(\zeta)=1$ if $\zeta\in(0,L_n]$ and zero elsewhere. The Fourier coefficients of $Q_p(\zeta)$ are given by

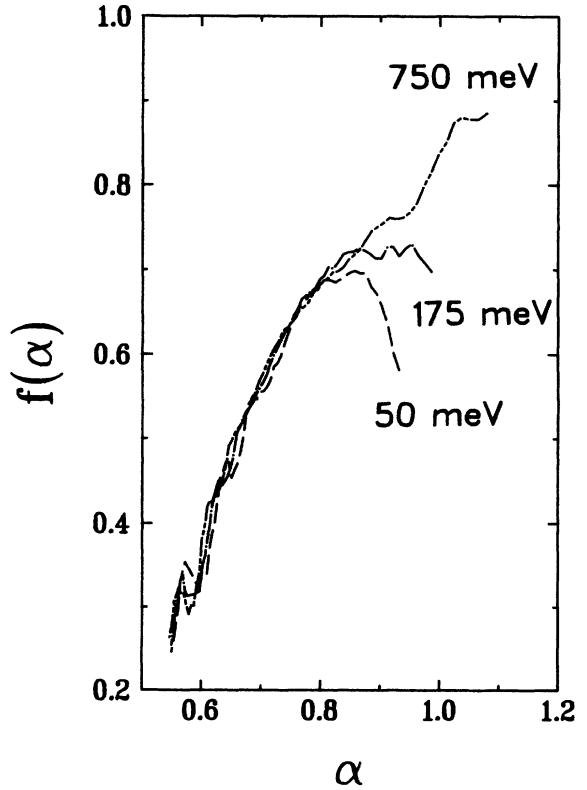

FIG. 9. $f(\alpha)$ as obtained from the data shown in Fig. 8 for bands between the ground state and the energy indicated.

$$c_l = \frac{1}{L}\int_0^L e^{ik_l\zeta}Q(\zeta)d\zeta = \frac{\sqrt{2\pi}}{L}Q(k_l) \equiv \sum_{n,m} c_{l_{nm}}, \tag{29}$$

where

$$c^*_{l_{nm}}c_{l_{nm}} = \frac{w^2}{a^2b^2}\left[\frac{\sin(p_{nm}w/2)}{p_{nm}w/2}\right]^2\left[\frac{\sin(k_l-k_{nm})L/2}{k_l-k_{nm}L/2}\right]^2 \tag{30}$$

with $k_l \equiv 2\pi l/L$, $w \equiv a\sin\theta + b\cos\theta$. The main peaks in $c_l^*c_l$ occur when l is a Fibonacci number F_i and $(n,m)=(F_{n'},F_{n'+1})$ in Eq. (30), so that the $\sin(x)/x$ functions are nearly 1. There are two major peaks between peaks F_{i+1} and F_{i+2}: The first comes from $(n,m)=2(F_{n'-1},F_{n'})$ and the second from $(n,m)=(F_{n'+1}+F_{n'-1},F_{n'+2}+F_{n'})$. Similarly, other peaks can be seen to be harmonics of Fibonacci peaks or to correspond to sums of Fibonacci numbers and their harmonics. The ratio between successive Fibonacci peaks in $c_l^*c_l$ is approximately τ^4, while $l \le F_k$ in the kth PA. This can be understood in terms of our geometric inflation picture. Going to the next Fibonacci number in l, and thus to the length scale of the next inflation, corresponds to a scaling of the 2D lattice by a factor of τ. This gives a factor of $\tau^4(1/\tau^2)$ for $c_l^*c_l$ from (30) in the new length scale. However, we have fixed L_n for which the factor $1/\tau^2$ overcompensates, giving a net τ^4. Roughly speaking, going to the next Fibonacci number corresponds to a scaling by τ in the linear dimensions of the embedding 2D lattice, giving a factor of τ^4 and not τ^2 as expected for a simple scaling in one dimension. The fact that this scaling is approximate is due to the $\sin(x)/x$ functions not being exactly 1 at a peak. We conjecture that the peaks of Fourier transforms of quasicrystals, corresponding to inflation scales, scale like their embedding periodic lattice if the Fourier transforms of the functions which select the weight with which a lattice site is projected are not themselves sharply peaked there.

Finally, we obtain the transform of the KP potential by convolving with the A and B pulses. If $V_A \neq V_B$, interference between the A and B lattices can destroy the scaling of the peaks. Figure 10 shows the exact gaps of the G lattice and compares them to the perturbative result. Main peaks match quite well and the cluster structure is qualitatively the same. For energies below approximately 100 meV the band structure of the G lattice scales itself approximately like E/τ^2.

All this leads to the following physical picture: Electrons see finer structure with increasing energy until the electron wavelength becomes smaller than an individual barrier. In the nth PA this occurs approximately when the band index exceeds F_n, the number of KP wells per unit cell. Bands within a cluster correspond to structure at roughly the same length scale, and a change in length scale, corresponding to an inflation transformation, appears as a main gap. To be explicit, the ground-state band ignores structure as well as it can, bands 1 and 2 see effectively one pulse each, and bands 3 and 4 form a mini cluster corresponding to inflation step AB. The next cluster sits at an energy where ABA is resolved, and so on. After each inflation step, the unit cell resolved by an

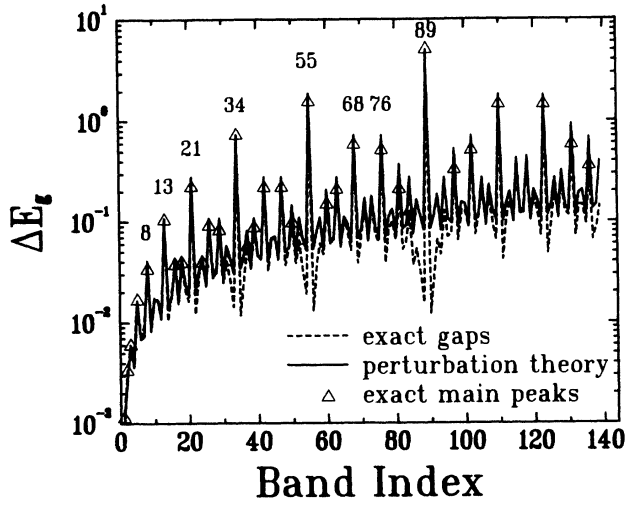

FIG. 10. Exact gaps and those obtained perturbatively vs band index for the 13th PA to the G lattice. For clarity, the main peaks of the exact result have been plotted as a triangle. The ratio between successive Fibonacci peaks is approximately τ^2.

electron has F_j equivalent pulses. The interaction amongst these gives F_j splittings forming the cluster at this energy (Fig. 11). Increasing the length of the unit cell by going to the next PA increases the number of equivalent pulses resolved at a cluster energy, and hence the number of bands per cluster, to the next Fibonacci number. This simple picture breaks down when interference between the A and B sublattices extinguishes a peak of the Fourier transform of $Q_p(\zeta)$ so that clusters may merge.

In the sense that the intracluster structure is a manifestation of the matrix dynamics [cf. Eq. (16)], it is not surprising than it resembles the structure of the tight-binding spectrum. In fact, Kohmoto showed[16] explicitly how to map a Schrödinger equation for any potential exactly onto a discrete tight-binding equation with energy-dependent coefficients.

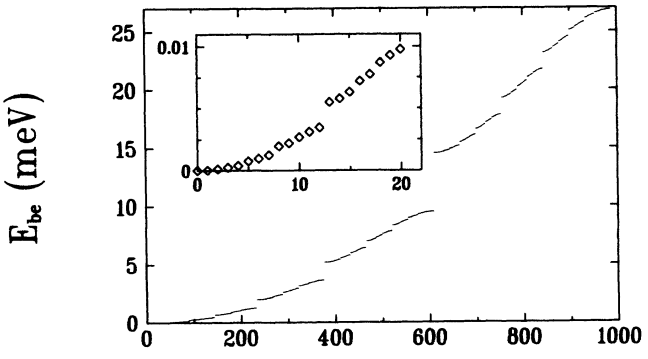

FIG. 11. The energy at the bottom edge of the bands vs band index for the $n=17$th PA to the G lattice. For large n, this figure is equivalent to a plot of energy vs integrated density of states. The inset shows the first few clusters of a Fibonacci number of bands.

The ground-state wave function is very similar to that of the exact two-cycle cluster edge of a constant-coefficient off-diagonal tight-binding model.[3] With increasing energy, the wave function of the center of the KP clusters changes from being dominated by the 2-cycle of the trace map to the fractal wave function of the 6-cycle. Furthermore, the nth band has n zeros at the bottom edge and $n+1$ zeros at the top edge, in accord with Schmidt's theorem[17] (Fig. 12). We noticed that zeros can be pinned by symmetry centers of the potential.

The obvious physical system to which the above results are applicable would be a superlattice where the unit cell of the nth PA is repeated a number of times so that Bloch boundary conditions are reasonably well satisfied. On the other hand, if the superlattice is an nth generation 1D quasicrystal (i.e., only one unit cell of the nth PA), and n is large enough so that the spectrum of the corresponding PA has converged beyond our experimental energy resolution, we are insensitive to boundary conditions and a cluster of states resolved as a single band will look exactly like a KP band of some appropriate lower PA. So in either case we essentially study a system equivalent to a

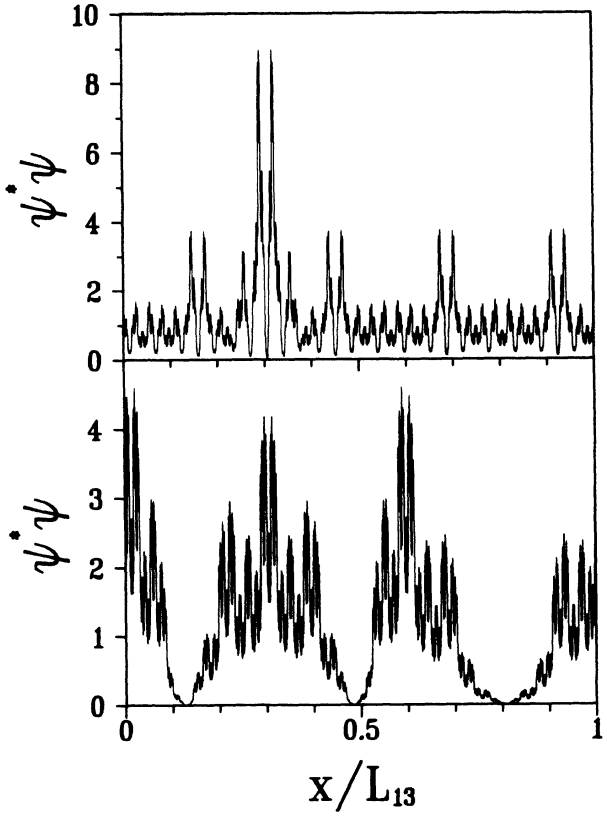

FIG. 12. Wave functions for the 13th PA to the G lattice. Energies are measured with respect to the free-electron ground state. The ground-state energy is 40.455 752 298 meV. They have been normalized so that $\int_0^L \psi^*\psi\, dx = 1$. Lower level: $E = 40.469\,444\,474$ meV. This is the bottom edge of band 3 at crystal momentum $K = \pi/L_{13}$. The wave function is basically a modulated 2-cycle showing three zeros in accord with Schmidt's theorem. Upper level: $E = 41.492\,589\,022$ meV. This is the center of the 27th band which is the center of the 21-band cluster. The fractal nature of the exact 6-cycle wave function is beginning to dominate (cf. Fig. 4).

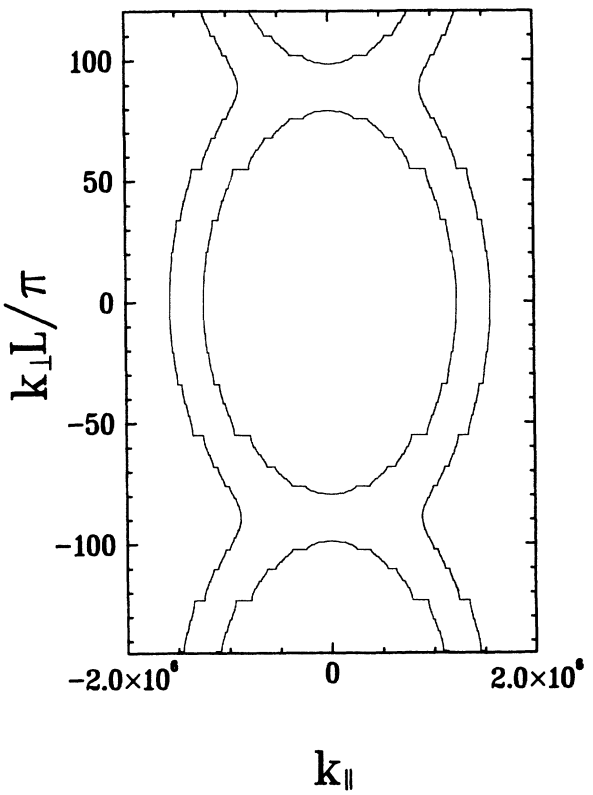

FIG. 13. Fermi surfaces of the 13th PA to the G lattice for $E_F=14$ meV, $n_e=1.27\times10^{17}$ cm^{-3} (open) and for $E_F=8.7$ meV, $n_e=6.31\times10^{16}$ cm^{-3} (closed).

PA. A Fermi surface is then clearly defined and given by $k_F^2=k_\parallel^2+k_\perp^2$. In Fig. 13 we show Fermi surfaces for the G lattice, in the 13th PA. The Fermi surface is open if the Fermi energy lies in a gap and closed if it cuts a band (cluster). For the parameters considered here, the gaps in the Fermi surface are seen to be very small and we expect it will be rather difficult to measure them in a standard Shubnikov–de Haas experiment. On the other hand, the parameter space of all possible Fibonacci lattices is very large and it might be possible to find parameters which would lead to experimentally accessible gaps.

Note added in proof. We have recently succeeded in finding the invariants of these maps and have identified their important cycles (unpublished).

ACKNOWLEDGMENTS

I am grateful to R. W. Cline for his support and his interest in this research. I would like to thank A. H. MacDonald and M. Plischke for useful discussions and encouragement. Further thanks go to W. N. Hardy and the University of British Columbia for financial support. This work was funded in part by the Natural Sciences and Engineering Research Council of Canada.

APPENDIX: DERIVATION OF THE PRECIOUS MEAN TRACE MAPS

Let M_k be a 2×2 matrix of unit determinant so that

$$\mathrm{Tr}M_k^n=\mathrm{Tr}M_k^{-n}=\lambda_k^n+\lambda_k^{-n}\ , \tag{A1}$$

where $M_k^{-n}\equiv(M_k^{-1})^n$ and λ_k is an eigenvalue of M_k. Choosing a basis in which M_q is diagonal, we see that

$$\mathrm{Tr}[M_p^m(M_q^n+M_q^{-n})]=(\lambda_q^n+\lambda_q^{-n})\,\mathrm{Tr}M_p^m=\mathrm{Tr}M_q^n\,\mathrm{Tr}M_p^m\ . \tag{A2}$$

Let

$$X_i\equiv(\mathrm{Tr}M_q)^{n-2i}$$

$$i\in\{0,1,\ldots,N\} \tag{A3}$$

$$Y_i\equiv\mathrm{Tr}M_q^{n-2i}-\delta_{n,2i}$$

where $N=\frac{1}{2}[n-(n\ \mathrm{mod}2)]$. It follows from the binomial theorem that

$$X_i=\sum_{j=0}^{N}C_{ij}Y_j\ , \tag{A4}$$

where

$$C_{ij}=\begin{cases}\begin{bmatrix}n-2i\\ j-i\end{bmatrix} & \text{if } j>i\ ,\\ 0 & \text{if } j<i\ .\end{cases} \tag{A5}$$

Note that the upper-triangular, $(N+1)\times(N+1)$ matrix C_{ij} has diagonal entries unity and is thus invertible:

$$\mathrm{Tr}M_q^n=\sum_{j=0}^{N}C_{0j}^{-1}(\mathrm{Tr}M_q)^{n-2j}\ . \tag{A6}$$

Now let M_k satisfy the precious mean recursion relation

$$M_{k+1}=M_{k-1}M_k^n\ . \tag{A7}$$

Equation (A1) implies

$$M_{k+1}^{n-1}M_{k-1}=M_{k+1}^nM_k^{-n}\ , \tag{A8}$$

$$M_k^{n-1}M_{k+2}=M_k^nM_{k+1}^n\ . \tag{A9}$$

The trace of the sum of the terms on the right-hand side (rhs) is of the form (A2); however, the sum of the lhs terms cannot be paired in this manner. We generate equations to pair of the lhs by multiplying (A8) and (A9) from the left by $M_{k+1}^{2(1-n)}$ and $M_k^{2(1-n)}$, respectively:

$$M_{k+1}^{1-n}M_{k-1}=M_{k+1}^{2-n}M_k^{-n}\ , \tag{A10}$$

$$M_k^{1-n}M_{k+2}=M_k^{2-n}M_{k+1}^n\ . \tag{A11}$$

Adding (A8)–(A11) we can pair all the lhs terms but not the rhs terms of (A10) and (A11). To pair these we add two more equations obtained by multiplying (A10) and (A11) from the left by $M_{k+1}^{2(n-2)}$ and $M_k^{2(n-2)}$, respectively. We continue this process of adding pairs of equations until their rhs (for n even) or their lhs (for n odd) is the power of a single matrix. Taking the trace of the sum of these equations we obtain

$$\sum_{l_{\text{odd}}=1}^{L}\{\mathrm{Tr}[M_{k-1}(M_{k+1}^{n-l}+M_{k+1}^{l-n})]+\mathrm{Tr}[M_{k+2}(M_k^{n-l}+M_k^{l-n})]-\delta_{n,l}(\mathrm{Tr}M_{k-1}+\mathrm{Tr}M_{k+2})\}$$
$$=\mathrm{Tr}[M_{k+1}^n(M_k^n+M_k^{-n})]+\sum_{r_{\text{even}}=2}^{R}\{\mathrm{Tr}[M_{k+1}^n(M_k^{n-r}+M_k^{r-n})]+\mathrm{Tr}[M_k^{-n}(M_{k+1}^{n-r}+M_{k+1}^{r-n})]$$
$$-\delta_{n,r}(\mathrm{Tr}M_{k+1}^n+\mathrm{Tr}M_k^{-n})\}\ , \tag{A12}$$

where $L=n-[(n+1)\,\mathrm{mod}2]$ and $R=n-(n\ \mathrm{mod}2)$. The paired terms then simplify by (A2) so that (A12) reads

$$\sum_{l_{\text{odd}}=1}^{L}[\mathrm{Tr}M_{k-1}\,\mathrm{Tr}M_{k+1}^{n-l}+\mathrm{Tr}M_{k+2}\,\mathrm{Tr}M_k^{n-l}-\delta_{n,l}(\mathrm{Tr}M_{k-1}+\mathrm{Tr}M_{k+2})]$$
$$=\mathrm{Tr}M_{k+1}^n\,\mathrm{Tr}M_k^n+\sum_{r_{\text{even}}=2}^{R}[\mathrm{Tr}M_{k+1}^n\,\mathrm{Tr}M_k^{n-r}+\mathrm{Tr}M_k^n\,\mathrm{Tr}M_{k+1}^{n-r}-\delta_{n,r}(\mathrm{Tr}M_{k+1}^n+\mathrm{Tr}M_k^n)]\ . \tag{A13}$$

The recursion relation for the traces is now obtained by writing traces of powers of matrices as powers of traces of matrices using (A6).

Equation (A13) shows that the recursion relation for the traces forms a 3D map for all n: $(x,y,z)\rightarrow(y,z,z'(x,y,z;n))$, where $x\equiv\frac{1}{2}\mathrm{Tr}M_{k-1}$, $y\equiv\frac{1}{2}\mathrm{Tr}M_k$, and $z\equiv\frac{1}{2}\mathrm{Tr}M_{k+1}$. Explicitly for $n=1$, 2, and 3,

$$z'(x,y,z;1)=2zy-x\ ,$$
$$z'(x,y,z;2)=\frac{1}{y}(4y^2z^2-y^2-z^2-xz)\ , \tag{A14}$$
$$z'(x,y,z;3)=\frac{1}{4y^2-1}(32y^3z^3-16yz^3-16y^3z-4xz^2+6yz+x)\ ,$$

Note that only the golden-mean trace map is volume conserving.

---

*Present address: Department of Physics, Simon Fraser University, Burnaby, British Columbia, Canada V5A 1S6.

[1]Stellan Ostlund, Rahul Pandit, David Rand, Hans Joachim Schellnhuber, and Eric D. Siggia, Phys. Rev. Lett. **50**, 1873 (1983).

[2]M. Kohmoto, L. P. Kadanoff, and C. Tang, Phys. Rev. Lett. **50**, 1870 (1983).

[3]Mahito Kohmoto, Bill Sutherland, and Chao Tang, Phys. Rev. B **35**, 1020 (1987).

[4]M. Kohmoto and Y. Oono, Phys. Lett. **102A**, 145 (1984).

[5]R. Merlin, K. Bajema, R. Clark, F.-T. Juang, and P. K. Bhattaacharya, Phys. Rev. Lett. **55**, 2915 (1985).

[6]J. Todd, R. Merlin, Roy Clarke, K. M. Mohanty, and J. D. Axe, Phys. Rev. Lett. **57**, 1157 (1986).

[7]M. W. C. Dharma-wardana, A. H. MacDonald, D. J. Lockwood, J.-M. Baribeau, and D. C. Houghton, Phys. Rev. Lett. **58**, 1761 (1987).

[8]H. L. Strömer, J. P. Eisenstein, A. C. Gossard, W. Wiegmann, and K. Baldwin, Phys. Rev. Lett. **56**, 85 (1986).

[9]For the construction of a generalized Penrose tiling in an arbitrary number of dimensions, see Michel Duneau and Andre Katz, Phys. Rev. Lett. **54**, 2688 (1985).

[10]R. K. P. Zia and W. J. Dallas, J. Phys. A **18**, L341 (1985).

[11]A. H. MacDonald, *Proceedings of the NATO Advanced Study Institute on Interfaces, Quantum Wells, and Superlattices, Banff, Alberta, Canada, 1987,* edited by C. Richard Leavens and Roger Taylor (Plenum, New York, in press).

[12]A. H. MacDonald and G. C. Aers, Phys. Rev. B **36**, 9142 (1987).

[13]Thomas C. Halsey, Morgens H. Jensen, Leo P. Kadanoff, Itamar Procaccia, and Boris I. Shraiman, Phys. Rev. A **33**, 1141 (1986).

[14]Mahito Kohmoto, Phys. Rev. A **37**, 1345 (1988).

[15]Mitchell J. Feigenbaum, Morgens H. Jensen, and Itamar Procaccia, Phys. Rev. Lett. **57**, 1503 (1986).

[16]M. Kohmoto, Phys. Rev. B **34**, 5043 (1986).

[17]E. H. Lieb and D. C. Mattis, in *Mathematical Physics in One Dimension,* edited by E. H. Lieb and D. C. Mattis (Academic, New York, 1966), p. 124.